The Astrophysical Journal, 670:968–977, 2007 December 1

THE WEBT CAMPAIGN ON THE BLAZAR 3C 279 IN 2006[1]

M. Böttcher,[2] S. Basu,[2] M. Joshi,[2] M. Villata,[3] A. Arai,[4] N. Aryan,[5] I. M. Asfandiyarov,[6] U. Bach,[3] R. Bachev,[7] A. Berduygin,[8] M. Blaek,[9] C. Buemi,[10] A. J. Castro-Tirado,[11] A. De Ugarte Postigo,[11] A. Frasca,[10] L. Fuhrmann,[12,13,3] V. A. Hagen-Thorn,[14] G. Henson,[15] T. Hovatta,[16] R. Hudec,[9] M. Ibrahimov,[6] Y. Ishii,[4] R. Ivanidze,[17] M. Jelínek,[11] M. Kamada,[4] B. Kapanadze,[17] M. Katsuura,[4] D. Kotaka,[4] Y. Y. Kovalev,[12,18] Yu. A. Kovalev,[18] P. Kubánek,[9] M. Kurosaki,[4] O. Kurtanidze,[17] A. Lähteenmäki,[16] L. Lanteri,[3] V. M. Larionov,[14] L. Larionova,[14] C.-U. Lee,[19] P. Leto,[20] E. Lindfors,[8] E. Marilli,[10] K. Marshall,[21] H. R. Miller,[21] M. G. Mingaliev,[22] N. Mirabal,[23] S. Mizoguchi,[4] K. Nakamura,[4] E. Nieppola,[16] M. Nikolashvili,[17] K. Nilsson,[8] S. Nishiyama,[4] J. Ohlert,[24] M. A. Osterman,[21] S. Pak,[25] M. Pasanen,[8] C. S. Peters,[26] T. Pursimo,[27] C. M. Raiteri,[3] J. Robertson,[28] T. Robertson,[29] W. T. Ryle,[21] K. Sadakane,[4] A. Sadun,[5] L. Sigua,[17] B.-W. Sohn,[19] A. Strigachev,[7] N. Sumitomo,[4] L. O. Takalo,[8] Y. Tamesue,[4] K. Tanaka,[4] J. R. Thorstensen,[26] G. Tosti,[13] C. Trigilio,[10] G. Umana,[10] S. Vennes,[28] S. Vitek,[11] A. Volvach,[30] J. Webb,[31] M. Yamanaka,[4] and H.-S. Yim[14]

Received 2007 July 6; accepted 2007 August 16

ABSTRACT

The quasar 3C 279 was the target of an extensive multiwavelength monitoring campaign from 2006 January through April. An optical-IR-radio monitoring campaign by the Whole Earth Blazar Telescope (WEBT) collaboration was organized around target-of-opportunity X-ray and soft γ-ray observations with *Chandra* and *INTEGRAL* in 2006 mid-January, with additional X-ray coverage by *RXTE* and *Swift* XRT. In this paper we focus on the results of the WEBT campaign. The source exhibited substantial variability of optical flux and spectral shape, with a characteristic timescale of a few days. The variability patterns throughout the optical *BVRI* bands were very closely correlated with each other, while there was no obvious correlation between the optical and radio variability. After the ToO trigger, the optical flux underwent a remarkably clean quasi-exponential decay by about 1 mag, with a decay timescale of $\tau_d \sim 12.8$ days. In intriguing contrast to other (in particular, BL Lac type) blazars, we find a lag of shorter wavelength behind longer wavelength variability throughout the *RVB* wavelength ranges, with a time delay increasing with increasing frequency. Spectral hardening during flares appears delayed with respect to a rising optical flux. This, in combination with the very steep IR-optical continuum spectral index of $\alpha_0 \sim 1.5$–2.0, may indicate a highly oblique magnetic field configuration near the base of the jet, leading to inefficient particle acceleration and a very steep electron injection spectrum. An alternative explanation through a slow (timescale of several days) acceleration mechanism would require an unusually low magnetic field of $B \lesssim 0.2$ G, about an order of magnitude lower than inferred from previous analyses of simultaneous SEDs of 3C 279 and other flat-spectrum radio quasars with similar properties.

Subject headings: galaxies: active — gamma rays: theory — quasars: individual (3C 279) — radiation mechanisms: nonthermal

Online material: color figures

[1] For questions regarding the availability of the data from the WEBT campaign presented in this paper, please contact the WEBT President Massimo Villata at villata@oato.inaf.it.

[2] Department of Physics and Astronomy, Astrophysical Institute, Clippinger 339, Ohio University, Athens, OH 45701.

[3] Istituto Nazionale di Astrofisica (INAF), Osservatorio Astronomico di Torino, Via Osservatorio 20, I-10025 Pino Torinese, Italy.

[4] Astronomical Institute, Osaka Kyoiku University, Kashiwara-shi, Osaka 582-8582, Japan.

[5] Department of Physics, University of Colorado at Denver, Campus Box 157, P. O. Box 173364, Denver, CO 80217-3364.

[6] Ulugh Beg Astronomical Institute, Academy of Sciences of Uzbekistan, 33 Astronomical Str., Tashkent 700052, Uzbekistan.

[7] Institute of Astronomy, Bulgarian Academy of Sciences, 72 Tsarigradsko Shosse Boulevard, 1784 Sofia, Bulgaria.

[8] Tuorla Observatory, University of Turku, 21500 Piikkiö, Finland.

[9] Astronomical Institute, Academy of Sciences of the Czech Republic, CZ-251 65 Ondrejov, Czech Republic.

[10] Osservatorio Astrofisico di Catania, Viale A. Doria 6, I-95125 Catania, Italy.

[11] Instituto de Astrofisica de Andalucia, Apartado de Correos, 3004, E-18080 Granada, Spain.

[12] Max-Planck-Institut für Radioastronomie, Auf dem Hügel 69, D-53121 Bonn, Germany.

[13] Osservatorio Astronomico, Università di Perugia, Via B. Bonfigli, I-06126 Perugia, Italy.

[14] Astronomical Institute, St. Petersburg State University, Universitetsky pr. 28, Petrodvoretz, 198504 St. Petersburg, Russia.

[15] Department of Physics, Astronomy, and Geology, East Tennessee State University and SARA Observatory, Box 70652, Johnson City, TN 37614.

[16] Metsähovi Radio Observatory, Helsinki University of Technology, Metsähovintie 114, 02540 Kylmälä, Finland.

[17] Abastumani Observatory, 383762 Abastumani, Georgia.

[18] Astro Space Center of Lebedev Physical Institute, Profsoyuznaya 84/32, Moscow 117997, Russia.

[19] Korea Astronomy and Space Science Institute, 61-1 Whaam-Dong, Yuseong-Gu, Daejeon 305-348, Korea.

[20] Istituto di Radioastronomia, Sezione di Noto, C. da Renna Bassa–Loc. Casa di Mezzo C. P. 141, I-96017 Noto, Italy.

[21] Department of Physics and Astronomy, Georgia State University, Atlanta, GA 30303.

[22] Special Astrophysical Observatory, Nizhnij Arkhyz, Karachai-Cherkessia 369167, Russia.

[23] Department of Astronomy, University of Michigan, 830 Dennison Building, Ann Arbor, MI 48109-1090.

[24] Michael Adrian Observatory, Astronomie-Stiftung Trebur, Fichtenstraße 7, D-65468 Trebur, Germany.

[25] Department of Astronomy and Space Science, Kyung Hee University, Seocheon, Gilheung, Yongin, Gyeonggi, 446-701, South Korea.

[26] Department of Physics and Astronomy, Dartmouth College, MS 6127, Hannover, NH 03755.

[27] Nordic Optical Telescope, Apartado 474, E-38700 Santa Cruz de La Palma, Santa Cruz de Tenerife, Spain.

[28] Florida Institute of Technology and SARA Observatory, 150 West University Boulevard, Melbourne, FL 32901-6975.

[29] Ball State University and SARA Observatory, Department of Physics and Astronomy, Munice, IN 47306.

[30] Crimean Astrophysical Observatory, Nauchny, Crimea 98409, Ukraine.

[31] Florida International University and SARA Observatory, University Park Campus, Miami, FL 33199.

1. INTRODUCTION

Flat-spectrum radio quasars (FSRQs) and BL Lac objects are active galactic nuclei (AGNs) commonly unified in the class of blazars. They exhibit some of the most violent high-energy phenomena observed in AGNs to date. Their spectral energy distributions (SEDs) are characterized by nonthermal continuum spectra with a broad low-frequency component in the radio–UV or X-ray frequency range and a high-frequency component from X-rays to γ-rays. Their electromagnetic radiation exhibits a high degree of linear polarization in the optical and radio bands and rapid variability at all wavelengths. Radio interferometric observations often reveal radio jets with individual components exhibiting apparent superluminal motion. At least episodically, a significant portion of the bolometric flux is emitted in >100 MeV γ-rays. Forty-six blazars have been detected and identified with high confidence in high-energy (>100 MeV) γ-rays by the Energetic Gamma-Ray Experiment Telescope (EGRET) instrument on board the *Compton Gamma Ray Observatory* (*CGRO*; Hartman et al. 1999; Mattox et al. 2001).

In the framework of relativistic jet models, the low-frequency (radio–optical/UV) emission from blazars is interpreted as synchrotron emission from nonthermal electrons in a relativistic jet. The high-frequency (X-ray–γ-ray) emission could be either produced via Compton upscattering of low frequency radiation by the same electrons responsible for the synchrotron emission (leptonic jet models; for a recent review see, e.g., Böttcher 2007a), or due to hadronic processes initiated by relativistic protons coaccelerated with the electrons (hadronic models; for a recent discussion see, e.g., Mücke & Protheroe 2001; Mücke et al. 2003).

The quasar 3C 279 ($z = 0.538$) is one of the best-observed FSRQs, not least because of its prominent γ-ray flare shortly after the launch of *CGRO* in 1991. It has been persistently detected by EGRET each time it was observed, even in its very low quiescent states, e.g., in the winter of 1992–1993, and is known to vary in γ-ray flux by roughly 2 orders of magnitude (Maraschi et al. 1994; Wehrle et al. 1998). It has been monitored intensively at radio, optical, and more recently also X-ray frequencies, and has been the subject of intensive multiwavelength campaigns (e.g., Maraschi et al. 1994; Hartman et al. 1996; Wehrle et al. 1998).

Also at optical wavelengths, 3C 279 has exhibited substantial variability over up to 2 orders of magnitude ($R \sim 12.5$–17.5). Variability has been observed on a variety of different timescales, from years down to intraday timescales. The most extreme variability patterns include intraday variability with flux decays of $\lesssim 0.1$ mag hr^{-1} (Kartaltepe & Balonek 2007). Observations with the *International Ultraviolet Explorer* in the very low activity state of the source in 1992 December–1993 January revealed the existence of a thermal emission component, possibly related to an accretion disk, with a luminosity of $L_{\rm UV} \sim 2 \times 10^{46}$ erg s^{-1} if this component is assumed to be emitting isotropically (Pian et al. 1999). Pian et al. (1999) also identified an X-ray spectral variability trend in archival *ROSAT* data, indicating a lag of $\sim$2–3 days of the soft X-ray spectral hardening behind a flux increase. Weak evidence for spectral variability was also found within the EGRET (MeV–GeV) energy range (Nandikotkur et al. 2007). At low γ-ray flux levels, an increasing flux seems to be accompanied by a spectral softening, while at high flux levels, no consistent trend was apparent.

The quasar 3C 279 was the first object in which superluminal motion was discovered (Whitney et al. 1971; Cotton et al. 1979; Unwin et al. 1989). Characteristic apparent speeds of individual radio components range up to $\beta_{\rm app} \sim 17$ (Cotton et al. 1979; Homan et al. 2003; Jorstad et al. 2004), indicating pattern flow speeds with bulk Lorentz factors of up to $\Gamma \sim 17$. Radio jet components have occasionally been observed not to follow straight, ballistic trajectories, but to undergo slight changes in direction between parsec and kiloparsec scales (Homan et al. 2003; Jorstad et al. 2004). VLBA polarimetry indicates that the electric field vector is generally well aligned with the jet direction on parsec to kiloparsec scales (Jorstad et al. 2004; Ojha et al. 2004; Lister & Homan 2005; Helmboldt et al. 2007), indicating that the magnetic field might be predominantly perpendicular to the jet on those length scales.

A complete compilation and modeling of all available SEDs simultaneous with the 11 EGRET observing epochs has been presented in Hartman et al. (2001a). The modeling was done using the time-dependent leptonic (SSC + EIC) model of Böttcher et al. (1997) and Böttcher & Bloom (2000) and yielded quite satisfactory fits for all epochs. The results were consistent with other model fitting works (e.g., Bednarek 1998; Sikora et al. 2001; Moderski et al. 2003) in concluding that the X-ray–soft γ-ray portion of the SED might be dominated by SSC emission, while the EGRET emission might require an additional, most likely external-Compton, component. The resulting best-fit parameters were consistent with an increasing bulk Lorentz factor, but decreasing Lorentz factors of the ultrarelativistic electron distribution in the comoving frame of the emission region during γ-ray high states, as compared to lower γ-ray states (Hartman et al. 2001a). However, such an interpretation also required changes of the overall density of electrons, and the spectral index of the injected electron power-law distribution, which did not show any consistent trend with γ-ray luminosity.

Hartman et al. (2001b) have investigated cross correlations between different wavelength ranges, in particular between optical, X-ray, and γ-ray variability. In that work, a general picture of a positive correlation between optical, X-ray, and γ-ray activity emerged, but no consistent trends of time lags between the different wavelength ranges were found.

The discussion above illustrates that, in spite of the intensive past observational efforts, the physics driving the broadband spectral variability properties of 3C 279 are still rather poorly understood. For this reason, W. Collmar et al. (2008, in preparation) proposed an intensive multiwavelength campaign in an optical high state of 3C 279, in order to investigate its correlated radio–IR–optical–X-ray–soft γ-ray variability. The campaign was triggered on 2006 January 5, when the source exceeded an *R*-band flux corresponding to $R = 14.5$. It involved intensive radio, near-IR (*JHK*), and optical monitoring by the Whole Earth Blazar Telescope (WEBT;[32] see, e.g., Raiteri et al. 2006; Villata et al. 2007 and references therein) collaboration through 2006 April, focusing on a core period of 2006 January and February. In order to illustrate the source's behavior leading up to the trigger in 2006 January, previously unpublished radio and optical data from late 2005 are also included in the analysis presented in this paper. X-ray and soft γ-ray observations were carried out by all instruments on board the *International Gamma-Ray Astrophysics Laboratory* (*INTEGRAL*) during the period of 2006 January 13–20. Additional, simultaneous X-ray coverage was obtained by *Chandra* and *Swift* XRT. These observations were supplemented by extended X-ray monitoring with the *Rossi X-Ray Timing Explorer* (*RXTE*). In this paper, we present details of the data collection, analysis, and results of the WEBT (radio–IR–optical) campaign. Preliminary results of the multiwavelength campaign have been presented in Collmar et al. (2007) and Böttcher (2007a, 2007b), and a final,

[32] See http://www.to.astro.it/blazars/webt.

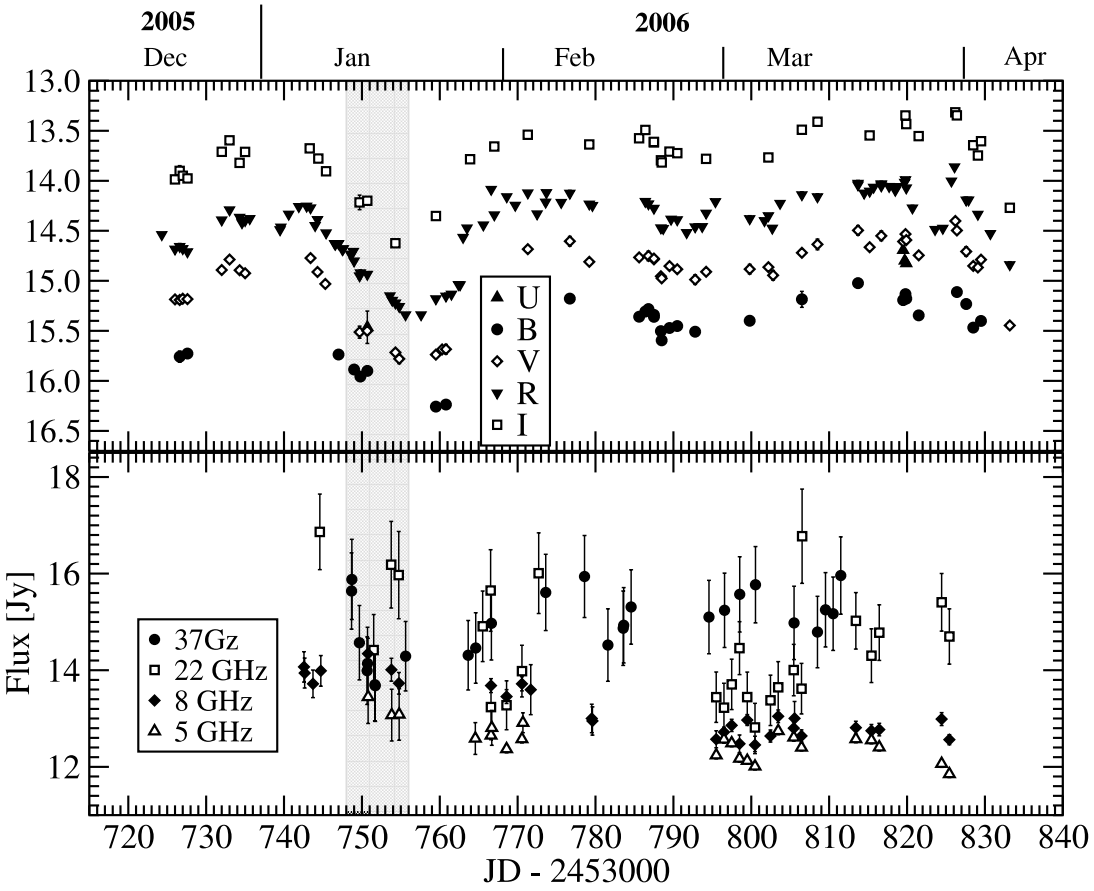

FIG. 1.—Timeline of the broadband campaign on 3C 279 in 2006, including the optical and radio light curves during the entire campaign period. The gray-shaded area indicates the period of the *INTEGRAL*, *Chandra*, and *Swift* observations. [*See the electronic edition of the Journal for a color version of this figure.*]

comprehensive report on the result of the entire multiwavelength campaign will appear in W. Collmar et al. (2008, in preparation).

Throughout this paper, we refer to α as the energy spectral index, F_ν [Jy] $\propto \nu^{-\alpha}$. A cosmology with $\Omega_m = 0.3$, $\Omega_\Lambda = 0.7$, and $H_0 = 70$ km s^{-1} Mpc^{-1} is used. In this cosmology, and using the redshift of $z = 0.538$, the luminosity distance of 3C 279 is $d_L = 3.1$ Gpc.

2. OBSERVATIONS, DATA REDUCTION, AND LIGHT CURVES

3C 279 was observed in a coordinated multiwavelength campaign at radio, near-IR, optical (by the WEBT collaboration), X-ray (*Chandra*, *Swift*, *RXTE* PCA, *INTEGRAL* JEM-X), and soft γ-ray (*INTEGRAL*) energies. The overall timeline of the campaign, along with the measured long-term light curves at radio and optical frequencies is illustrated in Figure 1. Simultaneous X-ray coverage with all X-ray/soft γ-ray telescopes mentioned above was obtained in the time frame January 13–20, as indicated by the gray-shaded area in Figure 1. Detailed results of those high-energy observations will be presented in W. Collmar et al. (2008, in preparation). Table 1 lists all participating observatories which contributed data to the WEBT campaign. In total, 25 ground-based radio, infrared, and optical telescopes in 12 countries on four continents contributed 2173 data points.

2.1. *Optical and Near-Infrared Observations*

The observing strategy and data analysis followed to a large extent the standard procedure for the optical data reduction for WEBT campaigns which is briefly outlined below. For more information on standard data reduction procedures for WEBT campaigns see also Villata et al. (2000, 2002, 2004a, 2004b), Raiteri et al. (2001, 2005), and Böttcher et al. (2003, 2005).

It had been suggested that, optimally, observers perform photometric observations alternately in the *B* and *R* bands, and include complete (*U*)*BVRI* sequences at the beginning and the end of each observing run. Exposure times should be chosen to obtain an optimal compromise between high precision (instrumental errors less than $\sim$0.03 mag for small telescopes and $\sim$0.01 mag for larger ones) and high time resolution. If this precision requirement leads to gaps of 15–20 minutes in each light curve, we suggest carrying out observations in the *R* band only. Observers were asked to perform bias and dark corrections, as well as flat-fielding on their frames, and obtain instrumental magnitudes, applying either aperture photometry (using IRAF or CCDPHOT) or Gaussian fitting for the source 3C 279 and four recommended comparison stars. This calibration has then been used to convert instrumental to standard photometric magnitudes for each data set. In the next step, unreliable data points (with large error bars at times when higher quality data points were available) were discarded. Our data did not provide evidence for significant variability on subhour timescales. Consequently, error bars on individual data sets could be further reduced by rebinning on timescales of typically 15–20 minutes. The data resulting at this stage of the analysis are displayed in Figure 1 (*top*).

In order to provide information on the intrinsic broadband spectral shape (and, in particular, a reliable extraction of $B - R$ color indices), the data were then dereddened using the Galactic

TABLE 1
List of Observatories that Contributed Data to the WEBT Campaign

Observatory	Specifications	Frequency/Filters	N_{obs}
Radio			
Metsähovi, Finland	14 m	37 GHz	70
Medicina, Italy	32 m	5, 8, 22 GHz	32
Noto, Italy	32 m	8, 22 GHz	6
RATAN-600, Russia	576 m (ring)	1, 2.3, 5, 8, 11, 22 GHz	138
Crimean Astr. Obs., Ukraine (RT-22)	22 m	36 GHz	7
Infrared			
Roque (NOT), Canary Islands	2.56 m	*J*, *H*, *K*	3
Optical			
Abastumani, Georgia (FSU)	70 cm	*R*	127
ARIES, Naintal, India		*R*	63
Belogradchik, Bulgaria	60 cm	*V*, *R*, *I*	75
BOOTES-1, Spain	30 cm	*R*	151
Catania, Italy	91 cm	*U*, *B*, *V*	33
Crimean Astr. Obs., Ukraine	70 cm	*B*, *V*, *R*, *I*	47
SMARTS, CTIO, Chile	90 cm	*B*, *V*, *R*	33
Kitt Peak (MDM), Arizona, USA	130 cm	*U*, *B*, *V*, *R*, *I*	190
Kitt Peak (MDM), Arizona, USA	240 cm	*R*	77
Michael Adrian Obs., Germany	120 cm	*R*	9
Mt. Lemmon, Arizona, USA	100 cm	*B*, *V*, *R*, *I*	214
Mt. Maidanak (AZT-22), Uzbekistan	150 cm	*B*, *V*, *R*, *I*	44
Osaka Kyoiku, Japan	51 cm	*V*, *R*, *I*	494
Roque (KVA), Canary Islands	35 cm	*R*	75
Roque (NOT), Canary Islands	256 cm	*U*, *B*, *V*, *R*, *I*	7
SARA, Arizona, USA	90 cm	*B*, *V*, *R*, *I*	242
Tenagra, Arizona, USA	81 cm	*B*, *V*, *R*, *I*	19
Torino, Italy	105 cm	*B*, *V*, *R*	3
Tuorla, Finland	103 cm	*R*	84

extinction coefficients of Schlegel et al. (1998) based on $A_B = 0.123$ mag and $E(B-V) = 0.029$ mag.[33]

Possible contaminations of the optical color information could generally also arise from contributions from the host galaxy and the optical–UV emission from an accretion disk around the central supermassive black hole in 3C 279. However, these contributions are not expected to be significant in the case of our campaign data: assuming absolute magnitudes of $M_V \sim -23$ and $M_B \sim -21$ for typical quasar host galaxies at $z \sim 0.5$ (e.g., Floyd et al. 2004; Zakamska et al. 2006), their contribution in the *V* and *B* band at the distance of 3C 279 would be $V_{gal} \sim 19.5$ and $B_{gal} \sim 21.6$, respectively. These are at least about 4 mag fainter than the actually measured total *B* and *V* magnitudes during our campaign, and thus negligible. The possible contribution of an accretion disk can be estimated on the basis of the thermal component for which Pian et al. (1999) found evidence in IUE observations during the 1992/1993 low state of 3C 279. Their best fit to this component suggests $U \sim 18.6$ and $B \sim 21$ (and much fainter contributions at lower frequencies), which corresponds to a contribution of $\lesssim 2.5$ % to the total *B* and *U* magnitudes measured during our campaign. Therefore, both the host galaxy and the accretion disk contribution are neglected in our further analysis.

The only infrared observations obtained for this campaign were one sequence of *JHK* exposures taken on 2006 January 15 with the 2.56 m NOT on Roque de los Muchachos on the Canary Island of La Palma. The resulting fluxes are included in the SED displayed in Figure 8.

[33] See http://nedwww.ipac.caltech.edu.

2.1.1. *Optical Light Curves*

The optical (and radio) light curves from 2005 December to 2006 April are displayed in Figure 1. The densest coverage was obtained in the *R* band, and the figure clearly indicates that the variability in the *B*, *V*, and *I* bands closely tracks the *R*-band behavior. The coverage in the *U* band was extremely sparse and does not allow any assessment of the *U*-band light curve during our campaign. Therefore, the *U* band is ignored in the following discussion, and we describe the main features of the variability behavior based on the *R*-band light curve.

The optical light curves show variability with magnitude changes of typically $\lesssim 0.5$ mag on timescales of a few days. The most notable exception to this relatively moderate variability is the major dip of the brightnesses in all optical bands right around our coordinated X-ray/soft γ-ray observations in 2006 January ($\approx$JD 2,453,742–2,453,770). In the *R* band, the light curve followed an unusually clean exponential decay over 1.1 mag in 13 days, i.e., a slope of $dR/dt = 0.085$ mag day^{-1} or a flux decay as $F(t) = F(t_0)e^{-(t-t_0)/\tau_d}$ with a decay constant of $\tau_d = 12.8$ days. Only moderate intraday deviations on a characteristic scale of $\lesssim 0.1$ mag day^{-1} are superposed on this smooth exponential decay.

In contrast to the smooth decline of the optical brightness during 2006 January 6–20, the subsequent rebrightening to levels comparable to those before the dip, appears much more erratic and involves a remarkably fast rise by $\sim$0.5 mag within $\sim$1 day

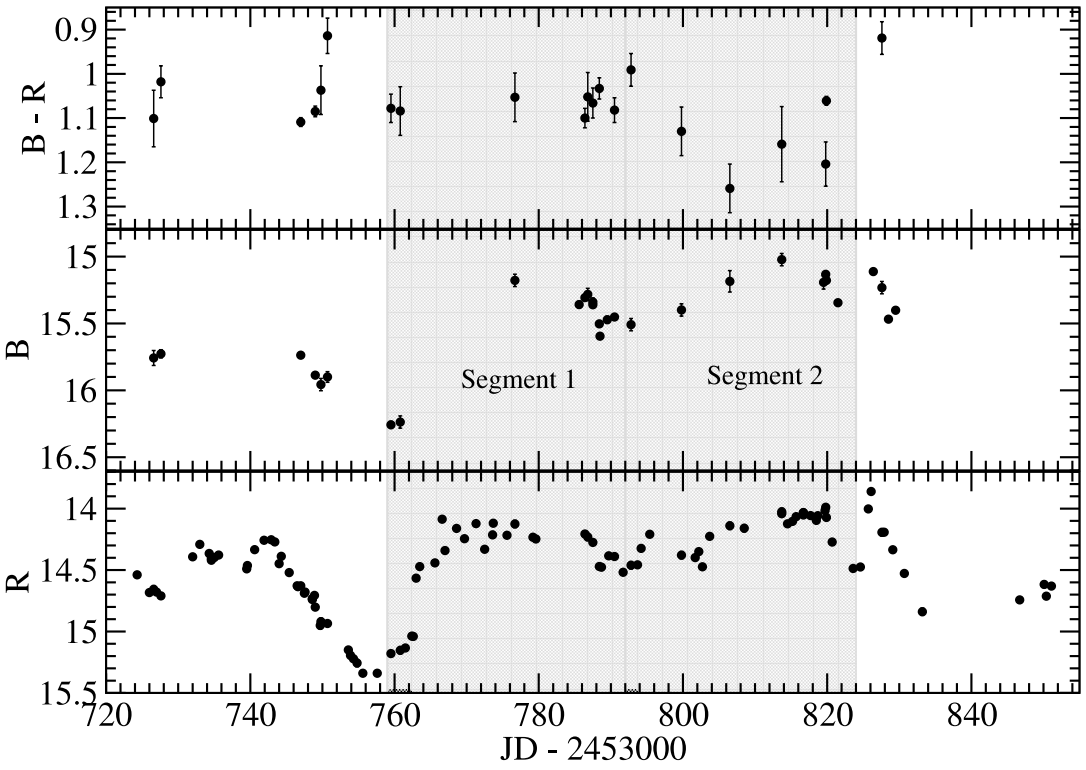

FIG. 2.—Light curve of the B and R magnitudes and the $B - R$ color index of 3C 279 over the duration of the entire campaign.

on January 27 (JD 2,453,763). Unfortunately, the detailed shape of this fast rise was not well sampled in our data set. If this was a quasi-exponential rise with a slope of $dR/dt \sim 0.5$ mag day^{-1}, it would correspond to a rise timescale of $\tau_r \sim 2.2$ days.

2.2. *Radio Observations*

At radio frequencies, 3C 279 was monitored using the 14 m Metsähovi Radio Telescope of the Helsinki University of Technology at 37 GHz; the 32 m radio telescope of the Medicina Radio Observatory near Bologna, Italy, at 5, 8, and 22 GHz; the 32 m antenna of the Noto Radio Observatory on Sicily, Italy, at 8 and 22 GHz; the 576 m ring telescope (RATAN-600) of the Russian Academy of Sciences at 1, 2.3, 5, 8, 11, and 22 GHz; and the 22 m RT-22 dish at the Crimean Astrophysical Observatory, Ukraine, at 36 GHz.

The Metsähovi data have been reduced with the standard procedure described in Teräsranta et al. (1998). The resulting 37 GHz light curve is reasonably well sampled during the period 2006 mid-January–mid-March. Inspection by eye in comparison to the optical light curves displayed in Figure 1 appears to indicate that the optical and 37 GHz light curves follow similar variability patterns with a radio lead before the optical variability by $\sim$5 days. However, a discrete cross-correlation analysis between the R-band and 37 GHz radio light curves did not reveal a significant signal to confirm this suggestion.

Also included in Figure 1 are the radio light curves at 5, 8, and 22 GHz. For details of the analysis of data from the Medicina and Noto radio observatories at those frequencies, see Bach et al. (2007). As already apparent in Figure 1, most of the data at frequencies below 37 GHz were not well sampled on the $\lesssim$3 months timescale of the 2006 campaign, and any evidence for variability did not show a discernable correlation with the variability at higher (radio and optical) frequencies.

All radio data contributed to this campaign are stored in the WEBT archive (see the WEBT Web site[34] for information regarding availability of the data). Radio data at all observed frequencies have been included in the quasi-simultaneous SED for 2006 January 15, shown in Figure 8. Given the generally very moderate radio variability at frequencies below 37 GHz, a linear interpolation between the two available data points nearest in time to 2006 January 15 was used to construct an estimate of the actual radio fluxes at that time.

3. OPTICAL SPECTRAL VARIABILITY

In this section we describe spectral variability phenomena, i.e., the variability of spectral (and color) indices and their correlations with monochromatic source fluxes. We concentrate here on the optical spectral variability as indicated by a change of the optical color. In particular, our observing strategy was optimized to obtain a good sampling of the $B - R$ color index as a function of time. Since our data did generally not indicate substantial flux changes on subhour timescales, we extracted $B - R$ color indices wherever both magnitudes were available within 20 minutes of each other. Figure 2 shows the $B - R$ color history over the entire campaign, compared to the B- and R-band light curves. Overall, there is no obvious correlation between the light curves and the color behavior of the source on long timescales. However, two short-term sequences attracted our attention: there is a sequence of brightness decline accompanied by a spectral hardening (declining $B - R$ index) around JD 2,453,750 (2006 January 14), and another sequence of a brightness increase accompanied by a spectral softening around JD 2,453,790–2,453,806 (February 23–March 11). However, we caution that incomplete

[34] See http://www.to.astro.it/blazars/webt.

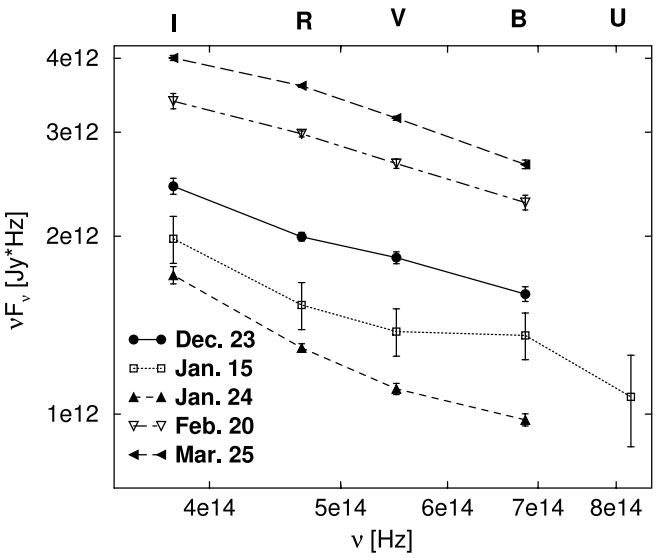

FIG. 3.—Snapshot optical (*BVRI*) continuum spectra for five epochs during our campaign. All measurements for each individual spectrum were taken within ≤20 minutes of each other. [*See the electronic edition of the Journal for a color version of this figure.*]

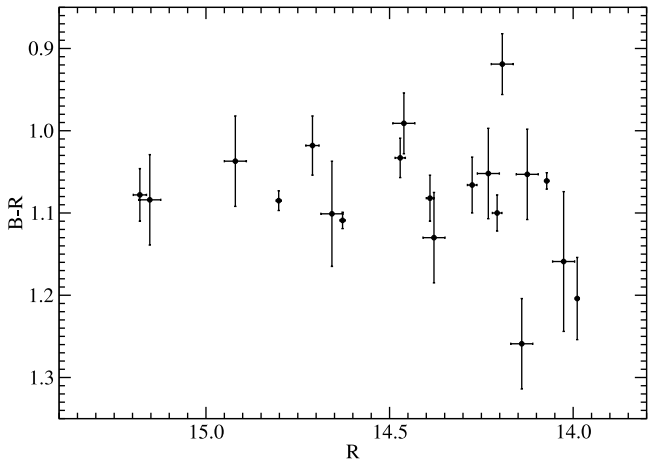

FIG. 4.—Color-magnitude diagram for the entire campaign period.

sampling, in particular in the *B* band, may introduce spurious effects.

A similar trend was recently observed in a multiwavelength WEBT campaign on the quasar 3C 454.3 (Villata et al. 2006), where it could be interpreted as a "little blue bump" due to the unresolved contribution from optical emission lines in the ∼2000–4000 Å wavelength range in the rest frame of the quasar, in particular from Fe II and Mg II (Raiteri et al. 2007). In order to test whether such an interpretation would also be viable in the case of 3C 279, we have compiled several simultaneous snapshot optical continuum (*BVRI*) spectra at various brightness levels (Fig. 3). All measurements for each individual spectrum displayed in Figure 3 have been taken within ≤20 minutes of each other. Only the spectrum of January 15 shows a significant deviation from a pure power law in the *B* band, and in that case there was simultaneous *U*-band coverage, which matched a straight power-law extrapolation of the *VRIJHK* spectrum. If the spectral upturn toward the blue end of the spectrum were due to an unresolved Mg II/Fe II line contribution, it should emerge even more clearly in the January 24 spectrum, which is characterized by a lower optical continuum flux level than the January 15 spectrum. Therefore, the compilation of spectra in Figure 3 does not provide any support for the existence of an essentially nonvariable continuum component at the blue end of the spectrum. For this reason, we believe that the color changes that we found in our data are in fact intrinsic to the blazar jet emission.

Figure 4 illustrates our impression from Figure 2 that there is no clear overall trend of source (*R* band) brightness with optical spectral hardness. However, the figure clearly illustrates that the scatter of the $B - R$ color index is significantly larger at larger source brightness, indicating that spectral variability is more likely to occur when the source is bright. Specifically, for $R > 14.5$, the data is consistent with a roughly constant value of $B - R = 1.09$, corresponding to a spectral index of $\alpha_0 = 1.9$ for a power-law continuum spectrum with $F_{\nu,0}[\mathrm{Jy}] \propto \nu^{-\alpha_0}$. At brightness levels $R < 14.5$, spectral variability by $\Delta(B - R) \lesssim 0.35$, corresponding to $\Delta\alpha_0 \lesssim 0.85$, is observed.

In Figure 5 we focus on two ∼1 month optical flares, around 2006 mid-January–mid-February and late February–late March, as indicated by the gray-shaded segments 1 and 2, respectively, in Figure 2. The number labels in the color-magnitude diagrams in Figure 5 indicate the time ordering of the points. While there is no obvious trend discernible in segment 1, segment 2 suggests the presence of a spectral hysteresis pattern: the spectral softening around JD 2,453,790–2,453,806 (February 23–March 11), mentioned above, precedes the main brightness increase. Subsequently, the optical continuum hardens while the source is still in a bright state. We need to caution that, due to the poor sampling of the *B*-band light curve during segment 2, the significance of the tentative hysteresis found here may be questionable. However, such hysteresis would naturally lead to a *B*-band time lag behind the *R* band, for which we do find evidence at 3.9 σ from a discrete correlation function analysis as described in the following section.

To our knowledge, such a spectral hysteresis has never been observed at optical wavelengths for any flat-spectrum radio quasar. It is reminiscent of the spectral hysteresis occasionally seen at X-ray energies in high-frequency peaked BL Lac objects (HBLs; e.g., Takahashi et al. 1996; Fossati et al. 2000; Kataoka et al. 2000). However, the spectral hysteresis observed in the X-rays of HBLs is generally clockwise (i.e., spectral hardening precedes flux rise; softening precedes flux decline), and can be interpreted as the synchrotron signature of fast acceleration of ultrarelativistic electrons, followed by a gradual decline on the radiative cooling timescale (e.g., Kataoka et al. 2000; Kusunose et al. 2000;

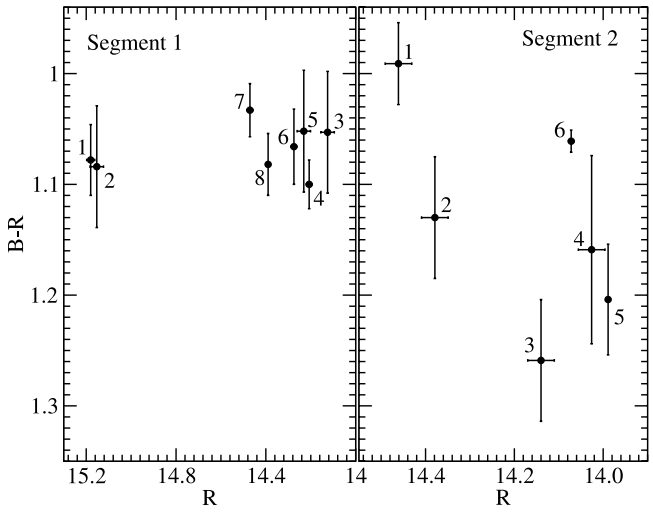

FIG. 5.—Color-magnitude diagrams for the two time segments marked in Fig. 2, with time ordering indicated by the numbers in the two panels.

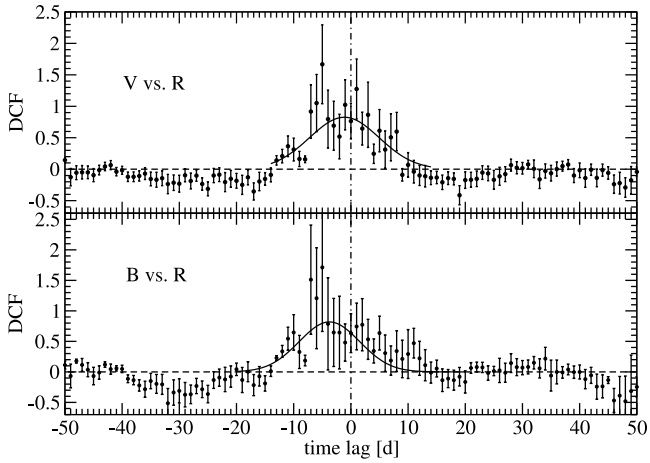

FIG. 6.—Discrete correlation functions between *V* and *R* (*top*), and *B* and *R* (*bottom*), respectively. The solid curves indicate the best fit with a symmetric Gaussian. This leads to a best-fit maximum correlation at $\tau_0 = (-1.14 \pm 0.48)$ days for the *V* band and $\tau_0 = (-3.75 \pm 0.96)$ days for the *B* band, indicating a lag of the *V*- and *B*-band light curves behind the *R* band.

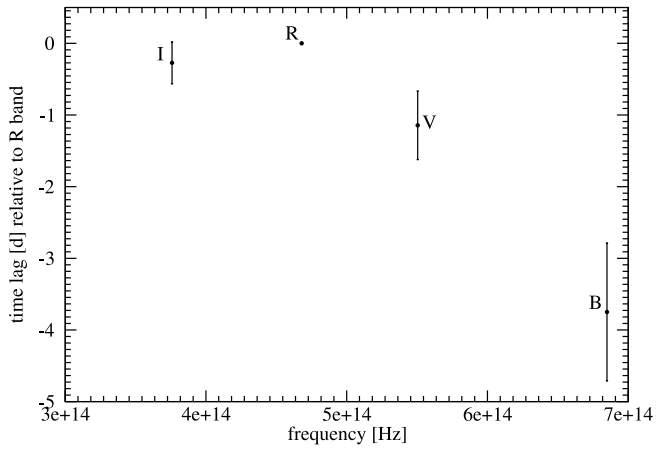

FIG. 7.—Best-fit time lag of the *R* band vs. *B*, *V*, *R*, and *I* bands, as a function of frequency.

Li & Kusunose 2000; Böttcher & Chiang 2002). In our case, the direction of the spectral hysteresis is counterclockwise (i.e., spectral softening precedes the flux rise; spectral hardening precedes flux decline). Possible physical implications of such hysteresis phenomena will be discussed in § 6.

4. INTERBAND CROSS-CORRELATIONS AND TIME LAGS

The result of an occasional counterclockwise hysteresis in 3C 279, as found in the previous section, immediately suggests the existence of a characteristic time lag of higher frequency behind lower frequency variability. In order to investigate this, we evaluated the discrete correlation function (DCF; Edelson & Krolik 1988) between the *R* band and the other optical light curves. In our notation, a positive value of the time lag $\Delta\tau$ would indicate a lag of the *R*-band light curve behind the comparison light curve. As mentioned earlier, the radio (and near-IR) light curves are too sparsely sampled and yielded no significant features in the DCF. Figure 6 shows the DCF between the *R* band and the *V* band (*top*) and the *B* band (*bottom*), using a sampling timescale of $\Delta\tau = 1$ days. We have done the same analysis using various other values of $\Delta\tau$, which yielded results consistent with the ones described below. We chose to show the results for $\Delta\tau = 1$ days because they provided the best compromise between dense timescale sampling and reduction of error bars.

The DCFs reveal clear correlations between the different optical wave bands, with peak values around 1. This confirms our previous impression from inspection by eye, that the variability patterns in all optical wave bands track each other very closely.

The resulting DCFs have then been fitted with a symmetric Gaussian, $F_0 e^{-(\tau-\tau_0)^2/(2\sigma^2)}$. This analysis yields nonzero offsets of the best-fit maxima, τ_0 at the ~ 3–$4\,\sigma$ level. Specifically, we find $\tau_0 = (-1.14 \pm 0.48)$ days for the *V* band and $\tau_0 = (-3.75 \pm 0.96)$ days for the *B* band. This indicates a hard time lag of higher frequency variability behind the variability at lower frequencies in the *B*–*V*–*R* frequency range. However, this trend does not continue into the *I* band. This is illustrated in Figure 7, where we plot the best-fit time lags as a function of photon frequency. However, we need to add a note of caution: the rather sparse sampling of the *B*- and *V*-band light curves leads to large error bars on the DCFs. Clearly, alternative, more complex representations, e.g., multiple Gaussians and/or asymmetric functions, will also provide acceptable fits to the observed DCFs and may lead to different quantitative results concerning the involved time lags. Future observations with denser *B*- and *V*-band sampling are needed in order to test the robustness of the trend found here.

The hard lag found in this analysis may be physically related to the ~ 2–3 day time lag of the soft X-ray spectral index behind the flux in *ROSAT* observations of 3C 279 in 1992 December–1993 January (Pian et al. 1999). Possible physical interpretations will be discussed in § 6.

5. BROADBAND SPECTRAL ENERGY DISTRIBUTION

The most complete broadband coverage of 3C 279 during our campaign was obtained on 2006 January 15. On that day, the only near-infrared (*JHK*) exposures were taken with the NOT, and simultaneous radio observations at 5, 8, 22, and 37 GHz were available as well. This is also within the time window of the X-ray and soft γ-ray observations, although in most cases, a meaningful extraction of spectral information required the integration over most of the high-energy observing period, 2006 January 13–20 (Collmar et al. 2007). The total snapshot SED composed of all available radio, near-IR, optical, X-ray, and soft γ-ray observations around 2006 January 15 is displayed in Figure 8, where all near-IR and optical data are taken within $\pm 1/2$ hr of UT 05:00 on January 15. The figure compares the 2006 January SED to previous SEDs from the bright flare during the first EGRET observing epoch in 1991 June, the low state of 1992 December/1993 January (both SEDs adapted from Hartman et al. 2001a), and a previous multiwavelength campaign around *INTEGRAL* AO-1 observations of 3C 279 in a low state in 2003 June (Collmar et al. 2004).

While the optical (presumably synchrotron) emission component clearly indicates that the source was in an elevated state compared to previous low states, the simultaneous X-ray–soft γ-ray spectrum is perfectly consistent with the low-state spectra of 1992/1993 and 2003. This is a very remarkable result and will be discussed in detail in a companion paper about the results of the entire multiwavelength campaign (W. Collmar et al. 2008, in preparation).

The NIR–optical continuum can be very well represented by a single power law with a spectral index of $\alpha_0 = 1.64 \pm 0.04$, corresponding to an underlying nonthermal electron distribution with a spectral index of $p = 4.28 \pm 0.08$, if the optical continuum is synchrotron emission. As already pointed out in Hartman et al. (2001a) for a comparison between various *EGRET* observing

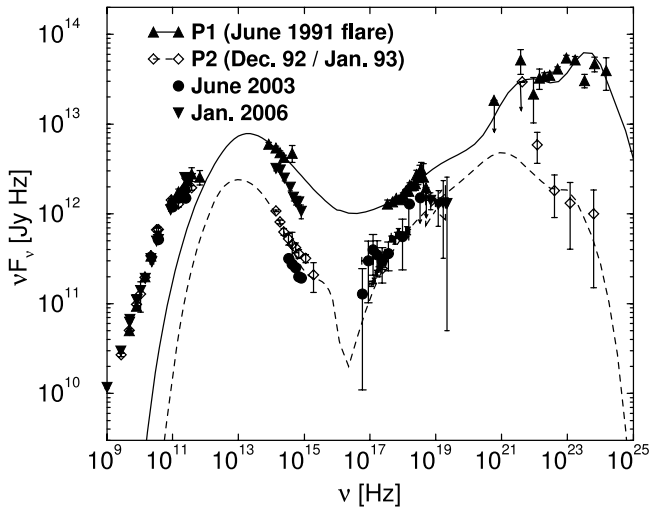

FIG. 8.—Simultaneous snapshot spectral energy distributions of 3C 279 at various epochs. Data pertaining to the multiwavelength campaign in 2006 January are plotted with red triangles. All IR and optical data were taken within ±1/2 hr of UT 05:00 on 2006 January 15; the X-ray and soft γ-ray data represent the time-averaged spectra throughout the respective observing windows in 2006 January, which included January 15 for all instruments. Model fits to the EGRET P1 and P2 SEDs are calculated using a time-dependent leptonic (SSC + EC) jet model, and taken from Hartman et al. (2001a). The 2003 June SED is from Collmar et al. (2004). [*See the electronic edition of the Journal for a color version of this figure*.]

epochs over ∼10 yr and confirmed by our campaign data on timescales of weeks–months (see § 3), the optical spectral index in 3C 279 does not show any systematic correlation with the brightness state of the source, and Figure 8 indicates that in our high-state observations of 2006, the continuum spectral slope is not significantly different from the slopes observed in the low states of 1992/1993 and 2003.

6. DISCUSSION

In this section, we discuss some general physical implications and constraints that our results can place on source parameters. In the following discussion we parameterize the magnetic field in units of Gauss, i.e., $B = 1B_{\rm G}$ Gauss, and the Doppler boosting factor $\mathrm{D} = (\Gamma[1 - \beta_\Gamma \cos\theta_{\rm obs}])^{-1}$ in units of 10, i.e., $\mathrm{D} = 10\mathrm{D}_1$, where Γ is the bulk Lorentz factor of the emitting region, $\beta_\Gamma c$ is the corresponding speed, and $\theta_{\rm obs}$ is the observing angle. The characteristic variability timescale is of the order of 1 to a few days, so we write $t_{\rm var}^{\rm obs} \equiv 1t_{{\rm var},d}^{\rm obs}$. In the same sense, we parameterize the time lag of the B band behind the R band as $\tau_{\rm BR}^{\rm obs} \equiv 1\tau_{{\rm BR},d}^{\rm obs}$ days with $\tau_{{\rm BR},d}^{\rm obs} \sim 3$. The observed variability timescale yields an estimate of the size of the emitting region, $R \equiv 10^{15}R_{15}$ cm through $R \lesssim c\mathrm{D}/(1+z)t_{\rm var}^{\rm obs}$. We find $R_{15} \lesssim 17\mathrm{D}_1 t_{{\rm var},d}^{\rm obs}$.

The (comoving) energies of electrons emitting synchrotron radiation at their characteristic peak frequencies in the R and B bands are

$$\gamma_R = 3.7\times10^3(B_{\rm G}\mathrm{D}_1)^{-1/2},$$
$$\gamma_B = 4.5\times10^3(B_{\rm G}\mathrm{D}_1)^{-1/2}. \quad (1)$$

The steep underlying electron spectrum with $p = 4.5$, inferred from the steep optical continuum, might indicate that the entire optical spectrum is produced by electrons in the fast-cooling regime. This implies that the radiative cooling timescale of electrons emitting synchrotron radiation in the optical regime is shorter than the characteristic escape timescale of those electrons. The respective timescales in the comoving frame, $t'_{\rm esc}$ and $t'_{\rm cool}$, can be written as

$$t'_{\rm esc} \equiv \eta\frac{R}{c} \lesssim 5.7\times10^5\eta\mathrm{D}_1 t_{{\rm var},d}^{\rm obs}\ {\rm s},$$
$$t'_{\rm cool} = \frac{\gamma}{\dot\gamma_{\rm rad}} \sim 7.7\times10^7 B_{\rm G}^{-1}\gamma^{-1}(1+k)^{-1}\ {\rm s}, \quad (2)$$

where $\eta \geq 1$ is the escape timescale parameter (as defined in the first line of eq. [2]), and k is a correction factor accounting for radiative cooling via Compton losses in the Thomson regime in a radiation field with an energy density $u'_{\rm rad} \equiv ku'_{\rm sy}$. Requiring that the cooling timescale is shorter than the escape timescale, at least for electrons emitting in the R band, leads to a lower limit on the magnetic field:

$$B \gtrsim B_c \equiv 1.3\times10^{-3}(1+k)^{-2}\eta^{-1}(t_{{\rm var},d}^{\rm obs})^{-2}\ {\rm G}, \quad (3)$$

which does not seem to pose a severe constraint, given the values of $B \sim$ a few G typically found for other FSRQs and also for 3C 279 from previous SED modeling analyses (e.g., Hartman et al. 2001a).

Another estimate of the comoving magnetic field can be found by assuming that the dominant portion of the time-averaged synchrotron spectrum is emitted by a power-law spectrum of electrons with $N_e(\gamma) = n_0 V_B \gamma^{-p}$ for $\gamma_1 \leq \gamma \leq \gamma_2$; here, V_B is the comoving blob volume, and we use $p = 4.5$ as a representative value inferred from the optical continuum slope. The normalization constant $n_0 = n_e(1-p)/(\gamma_2^{1-p} - \gamma_1^{1-p})$ is related to the magnetic field through an equipartition parameter $e_B \equiv u'_B/u'_e$ (in the comoving frame). Note that this equipartition parameter only refers to the energy density of the electrons, not accounting for a (possibly dominant) energy content of a hadronic matter component in the jet. Under these assumptions, the magnetic field can be estimated as described, e.g., in Böttcher et al. (2003). Taking the νF_ν peak synchrotron flux $f_\epsilon^{\rm sy}$ at the dimensionless synchrotron peak photon energy $\epsilon_{\rm sy} \equiv E_{\rm pk,sy}/(m_e c^2) \approx 3\times10^{-7}$ as $\sim10^{-10}$ erg cm^{-2} s^{-1}, we find

$$B \gtrsim B_{e_B} \equiv 1.86\mathrm{D}_1^{-13/7} e_B^{2/7}(t_{{\rm var},d}^{\rm obs})^{-1}\ {\rm G}. \quad (4)$$

This constitutes a more useful and realistic magnetic field estimate than equation (3). If, indeed, the optical emission is synchrotron emission from a fast-cooling electron distribution, then electrons have been primarily accelerated to a power-law distribution with an injection index of $q = p - 1 = 3.5$. This is much steeper than the canonical spectral index of $q \sim 2.2$–2.3 found for acceleration on relativistic, parallel shocks (e.g., Gallant et al. 1999; Achterberg et al. 2001), and could indicate an oblique magnetic field orientation (e.g., Ostrowski & Bednarz 2002; Niemiec & Ostrowski 2004), which would yield a picture consistent with the predominantly perpendicular magnetic field orientation observed on parsec scales (Jorstad et al. 2004; Ojha et al. 2004; Lister & Homan 2005). The observed hard lag (B vs. R) may then be the consequence of a gradual spectral hardening of the electron acceleration (injection) spectrum throughout the propagation of a relativistic shock front along the jet. Such a gradual hardening of the electron acceleration spectrum could be the consequence of the gradual build-up of hydromagnetic turbulence through the relativistic two-stream instability (see, e.g., Schlickeiser et al. 2002). This turbulence would harden the relativistic electron distribution via second-order Fermi acceleration processes (Virtanen &

Vainio 2005). Such a scenario would imply a length scale for the build-up of turbulence of

$$\Delta r \sim c\tau_{\rm BR}^{\rm obs} {\rm D}\Gamma/(1+z) \sim 5.6\times10^{-2}\tau_{{\rm BR},d}^{\rm obs}{\rm D}_1\Gamma_1 \sim 0.2 \ {\rm pc}$$

for the characteristic values of 3C 279.

Alternatively, the acceleration process could become more efficient along the jet if the magnetic field configuration gradually evolves into a more quasi-parallel one, on the same length scale of $\sim$0.2 pc as estimated above. However, this scenario might be in conflict with the predominantly perpendicular magnetic field orientation seen in the jets of 3C 279 on pc scales.

The hard lag in the optical regime may also be indicative of a slow acceleration mechanism, with an acceleration timescale of the order of the observed B versus R lag. This would imply an acceleration rate of

$$\dot\gamma_A \sim \frac{\gamma_B-\gamma_R}{\tau_{\rm BR}} \sim 6.8\times10^{-2}(\tau_{{\rm BR},d}^{\rm obs})^{-1}\left(\frac{{\rm D}_1}{B_{\rm G}}\right)^{1/2} \ {\rm s}^{-1}. \quad (5)$$

In this scenario, electrons could only be accelerated to at least γ_B if the acceleration rate of equation (5) is larger than the absolute value of the radiative (synchrotron + Compton) cooling rate corresponding to equation (2). This imposes an upper limit on the magnetic field:

$$B \lesssim B_{\rm acc} \sim 0.42{\rm D}_1^{1/3}(\tau_{{\rm BR},d}^{\rm obs})^{-2/3}(1+k)^{-2/3} \ {\rm G}. \quad (6)$$

This can be combined with the estimate in equation (4) to infer a limit on the magnetic field equipartition parameter:

$$e_B \lesssim e_{B,{\rm acc}} \sim 5.8\times10^{-3}{\rm D}_1^{23/3}(\tau_{{\rm BR},d}^{\rm obs})^{-7/3}(t_{{\rm var},d}^{\rm obs})^{7/2}(1+k)^{-7/3}. \quad (7)$$

Based on this equipartition parameter, one can use the magnetic field estimate of equation (4) to estimate the total amount of comoving energy contained in the emission region at any given time:

$$E_e' \sim \frac{4}{3}\pi R^3\frac{u_B'}{e_B} \sim 2.5\times10^{49}{\rm D}_1^{-4}\tau_{{\rm BR},d}^{\rm obs}(t_{{\rm var},d}^{\rm obs})^{-1/2}(1+k) \ {\rm erg}. \quad (8)$$

Assuming that the bulk of this energy is dissipated within the characteristic variability timescale, one can estimate the power in relativistic electrons in the jet:

$$L_{\rm jet} \sim \frac{E_e'}{t_{\rm var}'} \sim 4.5\times10^{43}{\rm D}_1^{-5}\tau_{{\rm BR},d}^{\rm obs}(t_{{\rm var},d}^{\rm obs})^{-3/2}(1+k) \ {\rm erg \ s}^{-1}. \quad (9)$$

Previous modeling works of the SEDs of FSRQs in general and 3C 279 in particular indicated characteristic magnetic field values of a few Gauss, in approximate equipartition with the ultrarelativistic electron population. The unusually low equipartition parameter in equation (7) could therefore pose a problem for the slow-acceleration scenario. Note, however, the very strong dependence of e_B on the Doppler factor ($\propto {\rm D}^{23/3}$). A Doppler factor ${\rm D} \sim 20$ could account for equipartition parameters of the order of 1. Also, the energy requirements of equations (8) and (9) seem reasonable, and there does not appear to be a strict argument that would rule this scenario out.

Another scenario one could think of would be based on a decreasing magnetic field along the blazar jet, leading to a gradually increasing cooling break in the underlying electron distribution. This would require that the cooling timescale for electrons emitting synchrotron radiation in the optical regime would be equal to or longer than the escape timescale. Thus, the inequality in equation (3) would be reversed. This would require unreasonably low magnetic fields. Furthermore, this scenario would be in conflict with the typically observed unbroken snapshot power-law continuum spectra throughout the optical-IR range. Therefore, this idea may be ruled out.

7. SUMMARY

We have presented the results of an optical-IR-radio monitoring campaign on the prominent blazar-type flat-spectrum radio quasar 3C 279 by the WEBT collaboration in 2006 January–April, around target-of-opportunity X-ray and soft γ-ray observations with *Chandra* and *INTEGRAL* in 2006 mid-January. Previously unpublished radio and optical data from several weeks leading up to the ToO trigger are also included.

The source exhibited substantial variability of flux and spectral shape, in particular in the optical regime, with a characteristic timescale of a few days. The variability patterns throughout the optical *BVRI* bands were very closely correlated with each other, while there was no significant evidence for a correlation between the optical and radio variability. After the trigger flux level for the *Chandra* and *INTEGRAL* ToOs was reached on 2006 January 5, the optical flux decayed smoothly by 1.1 mag within 13 days, until the end of the time frame of the X-ray and γ-ray observations. The decay could be well described by an exponential decay with a decay timescale of $\tau_d = 12.8$ days. The flux then recovered to approximately the predip values in a much more erratic way, including a $\sim$0.5 mag rise within $\sim$1 day.

A discrete correlation function analysis between different optical (*BVRI*) bands indicates a hard lag with a time delay increasing with increasing frequency, reaching $\sim$3 days for the lag of B behind R. This appears to be accompanied by a single indication of counterclockwise spectral hysteresis in a color-intensity diagram ($B-R$ vs. R). Thus, spectral hardening during flares appears delayed with respect to a rising optical flux. There is no consistent overall trend of optical spectral hardness with source brightness. However, our data indicate that the source displays a rather uniform spectral slope of $\alpha_0 \sim 1.9$ at moderate flux levels ($R > 14.5$), while spectral variability seems common at high flux levels ($R < 14.5$).

The occasional optical spectral hysteresis, in combination with the very steep IR-optical continuum spectral index of $\alpha_0 \sim 1.5$–2.0, may indicate a highly oblique magnetic field configuration near the base of the jet, leading to inefficient particle acceleration and a very steep electron injection spectrum. As the emission region propagates along the jet, a gradual hardening of the primarily injected ultrarelativistic electron distribution may be caused by the gradual build-up of hydromagnetic turbulence, which could lead to a gradually increasing contribution of second-order Fermi acceleration. This would imply a length scale of the build-up of hydromagnetic turbulence of $\Delta r \sim 0.2$ pc.

An alternative explanation of the hard lag may be a slow acceleration mechanism by which relativistic electrons are accelerated on a timescale of several days. However, even though this model can plausibly explain the observed variability trends and overall luminosity of the source, it requires an unusually low magnetic field in the emitting region of $B \lesssim 0.2$ G, unless rather

high Doppler factors of D20 are assumed. Such a small magnetic field would be about an order of magnitude lower than inferred from previous analyses of simultaneous SEDs of 3C 279 and other flat-spectrum radio quasars with similar properties.

The work of M. Böttcher and S. Basu was partially supported by NASA through *INTEGRAL* GO grant award NNG 06-GD57G and the *Chandra* GO program (administered by the Smithsonian Astrophysical Observatory) through award GO6-7101A. The Metsähovi team acknowledges the support of the Academy of Finland. Y. Y. K. is a research fellow of the Alexamder von Humboldt Foundation. RATAN-600 observations were partly supported by the Russian Foundation for Basic Research (project 05-02-17377). The St. Petersburg team was supported by the Russian Foundation for Basic Research through grant 05-02-17562.

REFERENCES

Achterberg, A., Gallant, Y. A., Kirk, J. G., & Guthmann, A. W. 2001, MNRAS, 328, 393
Bach, U., et al. 2007, A&A, 464, 175
Bednarek, W. 1998, A&A, 336, 123
Böttcher, M. 2007a, Ap&SS, in press (astro-ph/0608713)
———. 2007b, in ASP Conf. Ser. 373, The Central Engine of Active Galactic Nuclei, ed. L. C. Ho & J.-M. Wang (San Francisco: ASP), in press
Böttcher, M., & Bloom, S. D. 2000, AJ, 119, 469
Böttcher, M., & Chiang, J. 2002, ApJ, 581, 127
Böttcher, M., Mause, H., & Schlickeiser, R. 1997, A&A, 324, 395
Böttcher, M., et al. 2003, ApJ, 596, 847
———. 2005, ApJ, 631, 169
Collmar, W., et al. 2004, in Proc. 5th INTEGRAL Workshop, ed. B. Battrick (ESA SP-552; Noordwijk: ESA), 555
———. 2007, in Proc. 6th INTEGRAL Workshop, ed. S. Grebenev, R. Sunyaev, & C. Winkler (ESA SP-662; Noordwijk: ESA), in press
Cotton, W. D., et al. 1979, ApJ, 229, L115
Edelson, R. A., & Krolik, J. H. 1988, ApJ, 333, 646
Floyd, D. J. E., Kukula, M. J., Dunlop, J. S., McLure, R. J., Miller, L., Percival, W. J., Baum, S. A., & O'Dea, C. P. 2004, MNRAS, 355, 196
Fossati, G., et al. 2000, ApJ, 541, 166
Gallant, Y. A., Achterberg, A., & Kirk, J. G. 1999, A&AS, 138, 549
Hartman, R. C., et al. 1996, ApJ, 461, 698
———. 1999, ApJS, 123, 79
———. 2001a, ApJ, 553, 683
———. 2001b, ApJ, 558, 583
Helmboldt, J. F., et al. 2007, ApJ, 658, 203
Homan, D. C., Lister, M. L., Kellermann, K. I., Cohen, M. H., Ros, E., Zensus, J. A., Kadler, M., & Vermeulen, R. C. 2003, ApJ, 589, L9
Jorstad, S. G., Marscher, A. P., Lister, M. L., Stirling, A. M., Cawthorne, T. V., Gómez, J.-L., & Gear, W. K. 2004, AJ, 127, 3115
Kartaltepe, J. S., & Balonek, T. J. 2007, AJ, 133, 2866
Kataoka, J., Takahashi, T., Makino, F., Inoue, S., Madejski, G. M., Tashiro, M., Urry, C. M., & Kubo, H. 2000, ApJ, 528, 243
Kusunose, M., Takahara, F., & Li, H. 2000, ApJ, 536, 299
Li, H., & Kusunose, M. 2000, ApJ, 536, 729
Lister, M. L., & Homan, D. C. 2005, AJ, 130, 1389
Maraschi, L., et al. 1994, ApJ, 435, L91
Mattox, J. R., Hartman, R. C., & Reimer, O. 2001, ApJS, 135, 155
Moderski, R., Sikora, M., & Blazejowski, M. 2003, A&A, 406, 855
Mücke, A., & Protheroe, R. J. 2001, Astropart. Phys., 15, 121
Mücke, A., Protheroe, R. J., Engel, R., Rachen, J. P., & Stanev, T. 2003, Astropart. Phys., 18, 593
Nandikotkur, G., Jahoda, K. M., Hartman, R. C., Mukherjee, R., Sreekumar, P., Böttcher, M., Sambruna, R. M., & Swank, J. H. 2007, ApJ, 657, 706
Niemiec, J., & Ostrowski, M. 2004, ApJ, 610, 851
Ojha, R., Homan, D. C., Roberts, D. H., Wardle, J. F. C., Aller, M. F., Aller, H. D., & Hughes, P. A. 2004, ApJS, 150, 187
Ostrowski, M., & Bednarz, J. 2002, A&A, 394, 1141
Pian, E., et al. 1999, ApJ, 521, 112
Raiteri, C. M., et al. 2001, A&A, 377, 396
———. 2005, A&A, 438, 39
———. 2006, A&A, 459, 731
———. 2007, A&A, submitted
Schlegel, D. J., Finkbeiner, D. P., & Davis, M. 1998, ApJ, 500, 525
Schlickeiser, R., Vainio, R., Böttcher, M., Schuster, C., Lerche, I., & Pohl, M. 2002, A&A, 393, 69
Sikora, M., Blazejowski, M., Begelman, M. C., & Moderski, R. 2001, ApJ, 554, 1 (erratum 561, 1154)
Takahashi, T., et al. 1996, ApJ, 470, L89
Teräsranta, H., et al. 1998, A&AS, 132, 305
Unwin, S. C., Biretta, J. A., Hodges, M. W., & Zensus, J. A. 1989, ApJ, 340, 117
Villata, M., et al. 2000, A&A, 363, 108
———. 2002, A&A, 390, 407
———. 2004a, A&A, 421, 103
———. 2004b, A&A, 424, 497
———. 2006, A&A, 453, 817
———. 2007, A&A, 464, L5
Virtanen, J. J. P., & Vainio, R. 2005, ApJ, 621, 313
Wehrle, A. E., et al. 1998, ApJ, 497, 178
Whitney, A. R., et al. 1971, Science, 173, 225
Zakamska, N. L., et al. 2006, AJ, 132, 1496